Available online at www.sciencedirect.com
SCIENCE DIRECT®
Journal of Solid State Chemistry 177 (2004) 928–935
JOURNAL OF SOLID STATE CHEMISTRY
http://elsevier.com/locate/jssc

Structure of ten-layer orthorhombic $Ba_5Fe_5O_{14}$ ($BaFeO_{2.8}$) determined from single crystal X-ray diffraction

James L. Delattre,[a] Angelica M. Stacy,[a,*] and T. Siegrist[b]

[a] *Department of Chemistry, University of California at Berkeley, Berkeley, CA 94720, USA*
[b] *Bell Laboratories, Lucent Technologies, 600 Mountain Avenue, Murray Hill, NJ 07974, USA*

Received 31 July 2003; received in revised form 22 September 2003; accepted 24 September 2003

Abstract

The structure of the mixed-valent $Ba_5Fe_5O_{14}$ ($BaFeO_{2.8}$), prepared using a molten KOH–$Ba(OH)_2$ flux, has been determined using single crystal X-ray diffraction. $Ba_5Fe_5O_{14}$ forms twinned crystals with the orthorhombic space group *Cmcm*, $a = 5.7615(8)$, $b = 9.9792(14)$ and $c = 24.347(3)$ Å, $Z = 4$. The structure, which is closely related to the 10*H* $BaFeO_{2.65}$ perovskite, is composed of two oxygen-deficient BaO_2 layers and eight BaO_3 layers with a $(hchhc)_2$ stacking sequence, where *h* and *c* denote hexagonal or cubic layers. A displacement of barium and oxygen atoms in the BaO_2 layers from hexagonal special positions lowers the symmetry from hexagonal to orthorhombic. This combination of stacking and vacancies creates trimers of face-sharing FeO_6 octahedra pillared by dimers of corner-sharing FeO_4 tetrahedra. The Fe^{4+} atoms are located in the center of the trimer and in the tetrahedral sites. The magnetism of $Ba_5Fe_5O_{14}$, investigated using SQUID magnetometry, is characteristic of a strongly coupled antiferromagnet.

1. Introduction

The $BaFeO_x$ system, where $2.50 < x < 3.00$, has been studied extensively over the past 50 years, yet new insights into the rich structural chemistry of this system are still forthcoming [1–16]. While the entire series is related to the perovskite archetype, the members of the series are characterized by a number of different crystal systems—triclinic [4,17] monoclinic [10,15] orthorhombic [18], cubic [13], and most commonly hexagonal [2,9,12,16]. This structural variety can be attributed to several factors. First, these structures are typically derived from close packed BaO_3 layers that can be stacked in a cubic or hexagonal manner to give corner-sharing or face-sharing octahedral holes, respectively, that are occupied by iron atoms. Thus many stacking sequences [19] and therefore many unique iron-oxo networks are possible. This ordering of barium and iron atoms often leads to lower symmetry. Second, the number and location of oxygen vacancies may be different within each BaO_3 layer, which can lead to irregular coordination geometries or lower symmetry. Lastly, the preparative method greatly influences the previously described factors, stacking order and vacancy distribution, and in some cases can give new metastable phases.

The influential role of the synthetic route on the resulting structure is apparent if one considers the structures encountered for materials in the composition range $BaFeO_{2.52–2.65}$. If prepared from nitrates or carbonates, a mixture of monoclinic and orthorhombic phases is prevalent for $BaFeO_{2.52–2.54}$, only the orthorhombic phase is found for $BaFeO_{2.54–2.56}$ and a mixture of orthorhombic and 6-layered hexagonal (6*H*) phases form for $BaFeO_{2.56–2.65}$ [14]. However, Gomez et al. recently reported that compounds $BaFeO_{2.52–2.65}$, when prepared from the thermal decomposition of $Ba[Fe(CN)_5NO] \cdot 3H_2O$ under a flow of O_2, have a 10-layer hexagonal structure (10*H*) that tolerates a wide range of oxygen vacancy concentrations [16]. This new polytype is comprised of trimers of face-sharing octahedra that are pillared by corner-sharing tetrahedra. In theory, the 10*H* structure can accommodate the entire $BaFeO_{2.50–2.80}$ composition range, but materials in the highly oxidized $BaFeO_{2.65–2.80}$ end of the series have not been reported.

*Corresponding author. Department of Chemistry, University of California, Berkeley, 538A Latimer Hall, Berkeley, CA 94720, Fax: 510-642-8369.
E-mail address: astacy@socrates.berkeley.edu (A.M. Stacy).

0022-4596/$ - see front matter © 2003 Elsevier Inc. All rights reserved.
doi:10.1016/j.jssc.2003.09.032

Molten hydroxides are a useful medium for the growth of single crystals of transition metal oxides in high oxidation states [20], but only recently has this approach been used for the preparation of iron oxides. We have recently exploited the highly oxidizing conditions of molten hydroxides in the preparation of Fe^{4+} compounds, Ba_2FeO_4 and Ba_3FeO_5 [21]. Our efforts to extend this synthetic methodology to the mixed-valent perovskite-related barium iron oxides have yielded crystals of $Ba_5Fe_5O_{14}$, which are orthorhombic but closely related to the fully oxidized theoretical end-member of the $10H$ structure type. The structure was determined by single crystal X-ray diffraction and the magnetic properties were measured using SQUID magnetometry.

2. Experimental

2.1. Crystal growth

Anhydrous $Ba(OH)_2$ was prepared by dehydrating $Ba(OH)_2 \cdot 8H_2O$ (Strem, 98 + %) at 280°C for 1 h. Twinned crystals of $Ba_5Fe_5O_{14}$ were prepared by heating a mixture of 0.93 g $Ba(OH)_2$, 2.2 g of KOH (Johnson Mathey, Ultrapure) and 0.4 g of Fe_2O_3 (Alfa Aesar, 99.945%) mixed with 10 mL of NaOCl solution (Aldrich, available chlorine 10–13%) in a 20 mL alumina crucible capped with an alumina lid. The reaction mixture was heated from room temperature to 750°C over 6 h, maintained at 750°C for 5 h, and then slowly cooled to 600°C over a period of 40 h. The furnace was then shut off and the crucible and its contents were allowed to cool to room temperature. In the process of heating, the molten flux crept up the sides of the crucible and sealed the lid. Removal of the lid revealed a bed of loose crystals on the bottom of the crucible.

2.2. Structure determination

A black crystal of $Ba_5Fe_5O_{14}$ was fixed to the end of glass fiber and data were collected with a SMART CCD area detector. Data were integrated based on a primitive hexagonal cell with $a = 5.76$ and $c = 24.35$ Å, which is consistent with a structure derived from ten BaO_3 layers. A shape correction was applied using XPREP [22]. Then SADABS [23] was used to correction for absorption, including capillary absorption. An additional spherical absorption correction was applied using WinGX since SADABS created a pseudo-sphere with a diameter of 0.1 mm.

Based on the hexagonal metric of the unit cell and an indication of a c-glide in the systematic extinctions, $P6_3/mmc$ was assumed to be the most likely space group consistent with a 10-layer hexagonal close packed system. The three allowed stacking sequences [24] in $P6_3/mmc$, |(5)(5)|, |1(3)1|1(3)1|, and |2(1)2|2(1)2|, were investigated with the last giving the best results at $R_1 \cong 13\%$. Further analysis of the systematic extinctions, however, suggested the actual symmetry to be lower, with possible twinning present. As a starting point, a monoclinic cell with unique axis c and $\gamma = 120°$ was chosen, together with three-fold twinning. A solution was obtained in $P2_1/m$ with the three-fold twin operations resulting in $R_1 = 3.1\%$ and twin component volumes of 0.48/0.28/0.24. Further inspection of the monoclinic structural model revealed additional mirror and glide planes parallel to the long axis. Inclusion of these additional symmetry elements required a cell transformation to an orthorhombic cell with group symmetry $Cmcm$, a maximal non-isomorphous subgroup of $P6_3/mmc$ consistent with the possible orthohexagonal cell. Transformation of the original hexagonal cell to the C-centered orthorhombic cell was performed with the matrix, M

$$M = \begin{bmatrix} -1 & -1 & 0 \\ -1 & 1 & 0 \\ 0 & 0 & 1 \end{bmatrix}$$

giving unit cell parameters $a_0 = 5.67$, $b_0 = 9.98$, $c_0 = 24.35$ Å. The final cycle of full-matrix least-squares refinement, which included a three-fold twin law consistent with the 3 different orientations of the orthohexagonal cell, was based on 697 unique reflections and 54 parameters. Barium and iron atoms were refined anisotropically, while oxygen atoms were refined isotropically. Crystal data and details of the final refinement are given in Table 1. Atomic coordinates and isotropic displacement parameters are listed in Table 2. Anisotropic thermal displacement parameters are given in Table 3. Further details of the crystal structure investigation can be obtained from the Fachinformationszentrum Karlsruhe, 76344 Eggenstein-Leopoldshafen, Germany, (fax: (49) 7247-808-666; e-mail: crysdata@fiz.karlsruhe.de) on quoting the depository number CSD 391229.

2.3. Scanning electron microscopy/energy dispersive X-ray spectroscopy

Image collection and quantitative elemental microanalysis were performed with a JEOL 6300 scanning electron microscope equipped with an energy dispersive X-ray spectrometer.

2.4. Magnetic measurements

Magnetic susceptibility measurements were obtained as a function of temperature on a Quantum Design

MPMS SQUID. Data were collected on samples contained in gelatin capsules and corrected for the associated diamagnetism.

Table 1
Crystal data for $Ba_5Fe_5O_{14}$

Diffractometer	SMART CCD
Radiation	Moκ ($\lambda = 0.71069$ Å)
Crystal color, size	Black, $0.08 \times 0.06 \times 0.03$ mm
Crystal system, space group	Orthorhombic, *Cmcm*
Twin law	−1 1 0, −3 −1 0, 0 0 1
Unit cell dimensions	$a = 5.7615(8)$ Å, $\alpha = 90°$
	$b = 9.9792(14)$ Å, $\beta = 90°$
	$c = 24.347(3)$ Å, $\gamma = 90°$
Volume	1399.8(3) Å^3
Formula	$Ba_5Fe_5O_{14}$
Z, calculated density	4, 5.646 g/cm^3
Temperature	−168°C
Absorption coefficient	18.904 mm^{-1}
Formula weight	1189.95
Reflec. collected/unique	3142/697
Data/restraints/parameters	697/0/54
Reflection/parameter ratio	12.91
Goodness-of-fit on F^2	1.018
Final R indices ($I > 2.00\sigma(I)$)	$R_1 = 0.0267$, w$R_2 = 0.0702$
R indices (all data)	$R_1 = 0.0297$, w$R_2 = 0.0770$

3. Results and discussion

Molten hydroxide flux synthesis is a well established method for the growth of high-quality crystals of transition metal oxides, but this preparative method has to date not been applied to the $BaFeO_{3-x}$ system. This technique is well suited for the preparation of iron oxides in high (greater than +3) oxidation states, as the hydroxide solvent can simultaneously dissolve Fe^{3+} and oxidizers such as NaOCl and O_2, shifting the electrochemical potential in favor of Fe^{4+}. As the molten hydroxides gradually dehydrate, the solution saturates with O^{2-} and crystals precipitate. Using a molten KOH–$Ba(OH)_2$ eutectic flux, we have recently prepared black crystals of $Ba_5Fe_5O_{14}$ with a spindle-like habit. An SEM image of $Ba_5Fe_5O_{14}$ crystals is shown in Fig. 1. The Ba:Fe ratio 1:1 was confirmed using EDXS; while trace amounts of residual potassium and chlorine from the flux were detected during imaging, their respective signals were below detection limits when the electron beam was focused on a clean face.

Crystals grown by this method are of sufficient quality to determine the structure of $Ba_5Fe_5O_{14}$ by single crystal diffraction. The structure has an orthorhombic cell and is composed of two oxygen-deficient BaO_2 layers and eight stoichiometric BaO_3 layers. Using the stacking sequence descriptions [24,25] developed for hexagonal

Table 2
Atomic coordinates and equivalent isotropic displacement parameters (Å$^2 \times 10^3$) for $Ba_5Fe_5O_{14}$

	x	y	z	U_{eq}
Ba(1)	0.5000	0.8327(1)	0.0392(1)	0.014(1)
Ba(2)	0	0.9650(2)	0.2500	0.026(1)
Ba(3)	0.5000	0.1576(1)	0.1315(1)	0.016(1)
Fe(1)	0	0.9911(2)	0.1080(1)	0.013(1)
Fe(2)	0	0	0	0.012(1)
Fe(3)	0.5000	0.8213(2)	0.1790(1)	0.014(1)
O(1)	0.5000	0.8791(15)	0.2500	0.024(4)
O(2)	0	0.6760(14)	0.2500	0.011(3)
O(3)	0	0.8508(9)	0.0459(4)	0.015(3)
O(4)	0.7779(11)	0.0725(7)	0.0476(3)	0.014(2)
O(5)	0.7521(11)	0.8999(7)	0.1454(3)	0.017(2)
O(6)	0.5000	0.6429(9)	0.1581(5)	0.020(3)

U_{eq} is defined as one third of the trace of the orthogonalized U_{ij} tensor.

Table 3
Anisotropic displacement parameters (Å$^2 \times 10^3$) for $Ba_5Fe_5O_{14}$

	U_{11}	U_{22}	U_{33}	U_{23}	U_{13}	U_{12}
Ba_1	0.0137(8)	0.0133(8)	0.0141(4)	0.0002(4)	0.000	0.000
Ba_2	0.0241(9)	0.0405(9)	0.0130(6)	0.000	0.000	0.000
Ba_3	0.0142(7)	0.0135(7)	0.0189(5)	−0.0012(4)	0.000	0.000
Fe_1	0.0128(14)	0.0137(13)	0.0133(8)	0.0011(8)	0.000	0.000
Fe_2	0.0132(18)	0.0107(18)	0.0110(11)	0.0007(11)	0.000	0.000
Fe_3	0.0140(13)	0.0129(13)	0.0156(10)	−0.0007(8)	0.000	0.000

The anisotropic displacement factor takes the form: $\exp(-2\pi^2(a^{*2}U_{11}h^2 + b^{*2}U_{22}k^2 + c^{*2}U_{33}l^2 + 2a^*b^{*2}U_{12}hk + 2a^*c^{*2}U_{13}hl + 2b^*c^{*2}U_{23}kl))$.

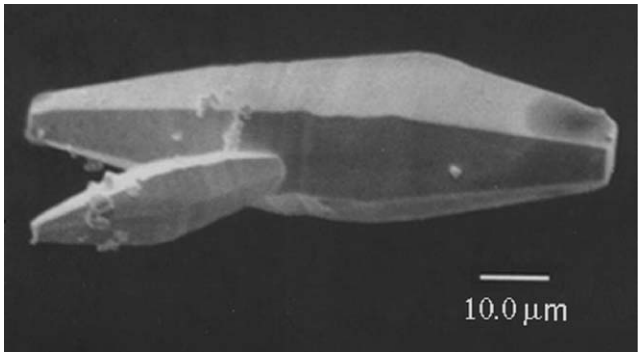

Fig. 1. SEM image of $Ba_5Fe_5O_{14}$ crystals.

perovskites, $Ba_5Fe_5O_{14}$ can be described as |2(1)2|2(1)2| in Zhdanov's notation, or $(hchhc)_2$ where *h* and *c* denote hexagonal or cubic layers. This 10-layer sequence has been reported for other oxygen-deficient perovskites such as $BaIr_{0.3}Co_{0.7}O_{2.83}$ [26], $BaFe_{0.8}Ni_{0.2}O_{2.70}$ [27] and $BaFeO_{2.52–2.65}$ [16].

The oxygen deficient layers in $BaFeO_{2.8}$ are hexagonal and lie between two cubic layers, creating a *chc* sequence. For a stoichiometric $BaMO_3$ perovskite, a *chc* sequence leads to two face sharing octahedra. In this case, the inclusion of a vacancy produces an *h*-BaO_2 layer that is no longer close-packed. The remaining two oxygen atoms rearrange in such a way that only one of them is within bonding distance of the two iron atoms adjacent to the layer, thus converting the face-sharing octahedra into corner-sharing tetrahedra. These tetrahedra also share corners with three trimers of face-sharing octahedra created by the *chhc* sequence of BaO_3 layers. Thus, the overall structure, shown in Fig. 2, can be viewed as stacks of trimers of face-sharing octahedra pillared by dimers of corner-sharing tetrahedra. An ORTEP diagram of the dimer–trimer stack is shown in Fig. 3. A list of relevant bond distances and bond angles is provided in Table 4.

One interesting structural aspect of the trimer is the size disparity between the face-sharing central and terminal octahedra. The average Fe1–O bond distance for the terminal octahedra is 2.01 Å, while the average Fe2–O bond distance for the central octahedron is 1.87 Å. This presents a minor problem because, if the octahedra are regular, the dimensions of the faces would be mismatched. Despite the size difference the central octahedron remains quite regular. This forces the terminal octahedra to distort considerably, reducing O–Fe–O bond angles from 90° to as small as 74.6° in order to accommodate the smaller shared face.

The tetrahedra that make up the dimer are also quite distorted with bond angles ranging from 104.1° to 124.3°. Here, the deviation from ideal tetrahedral coordination is likely due in part to stress associated with corner sharing with three trimers. However, the most deviant oxygen associated with Fe3 is O1, which is not shared with the trimers but with another tetrahedron. This oxygen is part of the BaO_2 layer, and may move from an ideal coordination geometry to improve the overall crystal packing within the layer, as the layer is not close-packed. The other oxygen atom in the BaO_2 layer, O2, is at a non-bonding distance of 3.66 Å from Fe3, the nearest iron atom. Instead it is coordinated by five barium atoms; three at 2.88–2.89 Å and two with longer contacts at 3.57 Å.

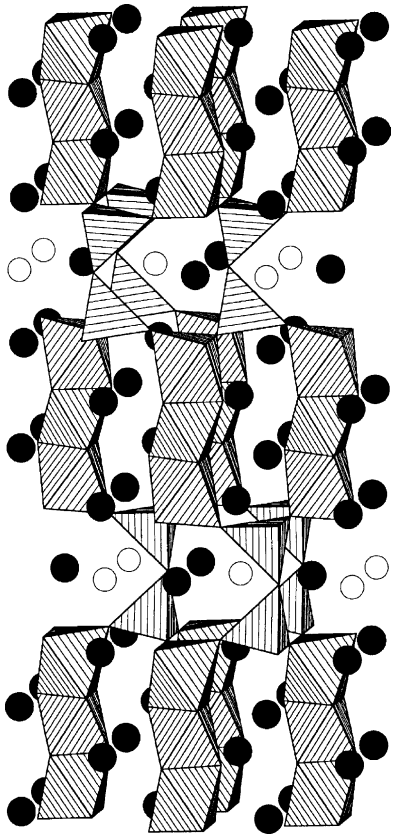

Fig. 2. Structure of $Ba_5Fe_5O_{14}$ viewed approximately along the [010] axis. Barium atoms are shown in black and oxygen atoms not bonded to iron are shown in white.

With the aid of high quality structural data, it is often possible to determine the oxidation state for each transition metal ion in a mixed-valent compound. For $Ba_5Fe_5O_{14}$ the average iron oxidation state is +3.6 and therefore one would expect three Fe^{4+} sites and two Fe^{3+} sites per five iron atoms. The relative multiplicities for Fe1, Fe2 and Fe3 are 2, 1 and 2, respectively, and therefore Fe2 must have an oxidation state of +4 if 3/5 of the iron atoms are tetravalent. This corresponds to Fe^{4+} on the inversion center of the face-sharing trimer. This assertion is consistent with the crystallographic data, as the average Fe2–O bond distance is 1.87 Å, considerably shorter than the average Fe^{3+}–O distance of 2.00 Å determined by Shannon [28]. However, the

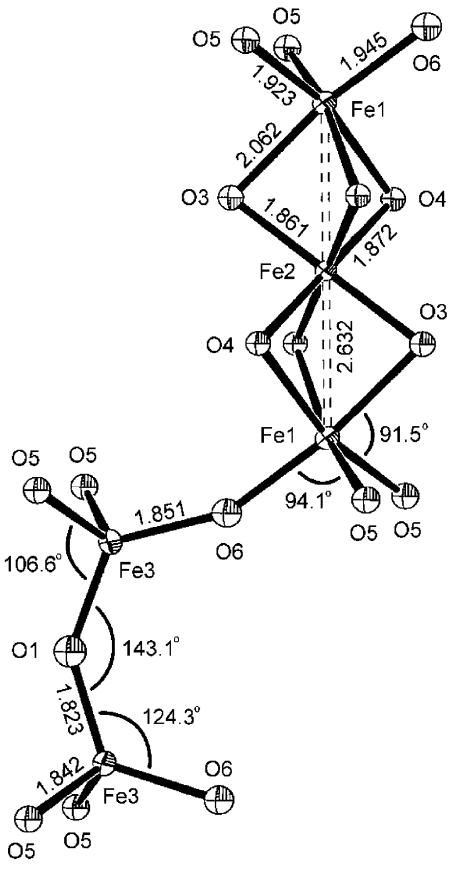

Fig. 3. ORTEP diagram of the iron-oxo network.

average Fe1–O bond distance for the terminal octahedra is 2.01 Å, which suggests that the oxidation state for Fe1 is +3. In order to achieve charge balance, tetrahedral Fe3 must therefore be tetravalent. The short average Fe3–O bond distance of 1.84 Å is consistent with Fe^{4+}; in fact, we have recently found FeO_4^{4-} tetrahedra in Ba_3FeO_5 have an average Fe–O bond distance of 1.84 Å. Thus the trimers can be viewed as $Fe_3O_{12}^{14-}$ units with a central Fe^{4+} and terminal Fe^{3+} atoms, while the dimers can be viewed as $Fe_2O_7^{6-}$ units containing only Fe^{4+}. A similar oxidation state distribution has been reported for 5*H* $BaVO_{2.8}$ [29], which likewise contains trimers of face sharing octahedra and corner-sharing tetrahedra, though in this case only three of the four tetrahedral corners are shared. Still, the 4-coordinate vanadium atoms and the vanadium atoms in the central octahedron of the trimer are tetravalent, while the vanadium atoms at the trimer termini are trivalent.

The distance between [Ba,O] layers varies depending upon the characteristics of the Fe atoms sandwiched between the layers. As we noted earlier, the central Fe2 octahedron of the dimer is smaller than the terminal octahedra because Fe2 is oxidized. This creates a compression of the two $[(Ba1)_1(O3)_1(O4)_2]$ layers adjacent to Fe2, which leads to an interlayer thickness

Table 4
Selected interatomic bond distances (Å) and bond angles (°) for $Ba_5Fe_5O_{14}$

$(Ba1)O_{11}$	
Ba(1)–O(3)	2.765(10)
Ba(1)–O(4) × 2	2.816(7)
Ba(1)–O(4) × 2	2.886(7)
Ba(1)–O(3) × 2	2.8909(9)
Ba(1)–O(4) × 2	2.902(7)
Ba(1)–O(5) × 2	3.041(7)
$(Ba2)O_9$	
Ba(2)–O(6) × 2	2.855(11)
Ba(2)–O(2)	2.884(14)
Ba(2)–O(5) × 4	2.990(7)
Ba(2)–O(1) × 2	3.005(4)
$(Ba3)O_{10}$	
Ba(3)–O(4) × 2	2.730(6)
Ba(3)–O(5) × 2	2.829(7)
Ba(3)–O(3)	2.841(10)
Ba(3)–O(2)	2.8908(12)
Ba(3)–O(6) × 2	2.957(3)
Ba(3)–O(5) × 2	2.972(7)
$(Fe1)O_6$	
Fe(1)–O(5) × 2	1.923(7)
Fe(1)–O(6)	1.945(10)
Fe(1)–O(3)	2.062(10)
Fe(1)–O(4) × 2	2.112(7)
O(3)–Fe(1)–O(4)	75.5(2)
O(4)–Fe(1)–O(4)	74.6(4)
O(5)–Fe(1)–O(5)	95.9(4)
O(5)–Fe(1)–O(6)	94.1(3)
O(5)–Fe(1)–O(3)	91.5(3)
O(5)–Fe(1)–O(4)	164.1(3)
O(5)–Fe(1)–O(4)	93.5(3)
O(6)–Fe(1)–O(4)	97.9(3)
O(6)–Fe(1)–O(3)	171.6(4)
(Fe2)O6	
Fe(2)–O(3) × 2	1.861(9)
Fe(2)–O(4) × 4	1.872(6)
O(3)–Fe(2)–O(3)	180.0(6)
O(3)–Fe(2)–O(4)	93.6(3)
O(3)–Fe(2)–O(4)	86.4(3)
O(4)–Fe(2)–O(4)	86.2(4)
O(4)–Fe(2)–O(4)	180.0(5)
O(4)–Fe(2)–O(4)	93.8(4)
Fe(1)–Fe(2)	2.6315(17)
Fe(1)–Fe(2)–Fe(1)	180.00(7)
(Fe3)O4	
Fe(3)–O(1)	1.823(5)
Fe(3)–O(5) × 2	1.842(7)
Fe(3)–O(6)	1.851(10)
O(1)–Fe(3)–O(5)	106.6(3)
O(1)–Fe(3)–O(6)	124.3(6)
O(5)–Fe(3)–O(5)	104.1(5)
O(5)–Fe(3)–O(6)	106.8(3)
Fe(3)–O(6)–Fe(1)	157.0(6)
Fe(3)–O(1)–Fe(3)	143.1(9)

of 2.185 Å. These layers are quite close to one another, considering that the average layer thickness is 2.435 Å, based on the c lattice parameter. The interlayer distance between $[(Ba1)_1(O3)_1(O4)_2]$ and $[(Ba3)_1(O5)_2(O6)_1]$ layers, the layers adjacent to Fe1, is 2.434 Å; very close to the average. Tetrahedral Fe3 appears to have a pillaring effect on the adjacent layers, as the $[(Ba3)_1(O5)_2(O6)_1]$ layer and defect layer $[(Ba2)_1(O1)_1(O2)_1]$ are separated by 2.554 Å. This is to be expected, as the $M\cdots M$ distance between two face-sharing octahedra is shorter than the $M\cdots M$ distance in a M–O–M unit, unless the M–O–M bond angle approaches 90°, which is not the case here.

The stoichiometries of the BaO_x layers varies more widely in orthorhombic $BaFeO_{2.8}$ than in related $BaFeO_{3-x}$ compounds. For example, Jacobson has reported that hexagonal and cubic layers have the compositions $BaO_{2.50}$ and $BaO_{2.835}$, respectively, in 6H $BaFeO_{2.79}$ [9]. The vacancy distribution in $BaFeO_{2.8}$ is more similar to that of 10H $BaFeO_{2.65}$ in that both compounds have $BaO_{2.0}$ and $BaO_{3.0}$ layers that give rise to the dimer-trimer structure discussed earlier. However, 10H $BaFeO_{2.65}$ also contains $BaO_{2.63}$ layers with disordered vacancies [16]. Thus, $BaFeO_{2.8}$ can be viewed as the end member the 10H $BaFeO_{2.8-\delta}$ polytype, as it has the same stacking sequence but no randomly distributed vacancies. The wide variance in oxygen vacancies from layer-to-layer, as is observed in 10H $BaFeO_{2.65}$ and orthorhombic $BaFeO_{2.8}$, appears to be a consequence of the relatively low temperatures used in their preparation. These phases do not appear to be accessible through traditional high temperature routes [30] and may therefore be considered kinetic (metastable) products at room temperature.

Most layered perovskites described in the literature are hexagonal, but $Ba_5Fe_5O_{14}$ contains several structural peculiarities that lead to orthorhombic symmetry. The lowered symmetry can be attributed to the oxygen deficient BaO_2 layers, located on mirror planes at $z = 1/4$ and 3/4. A schematic of the orthorhombic BaO_2 layer in *Cmcm* superimposed on a hexagonal BaO_2 layer in $P6_3/mmc$ as viewed from the [001] direction is shown in Fig. 4. Orthorhombic barium atoms are shown in black, orthorhombic oxygen atoms are shown in gray, and their hexagonal analogs are shown as white circles. The layers are drawn so that their a axes coincide. With the symmetry lowered from $P6_3/mmc$ to *Cmcm*, the barium and oxygen atomic coordinates are free to move away from the 6-bar axes during refinement. For Ba2, a displacement of 0.35 Å in the $-b$ direction from the $0, 0, 1/4$ position was observed. On the other hand, O1, which bridges the tetrahedra, moved 0.39 Å in the $+b$ direction, while O2 moved very little. Furthermore, the thermal parameters of all these atoms improved significantly. Considering the close relationship between the 10H and orthorhombic structures, it is likely that the crystal grew in hexagonal symmetry at higher temperatures, but underwent twinning upon cooling due to a phase transition to orthorhombic symmetry associated with oxygen vacancy ordering.

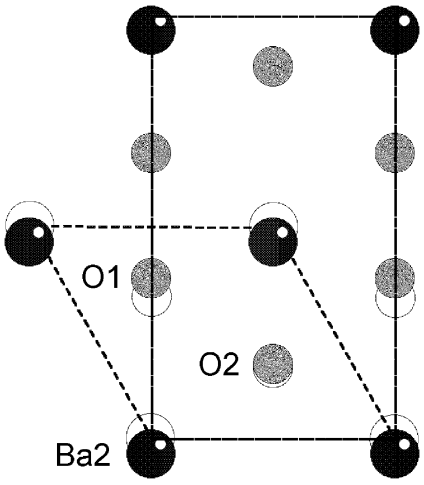

Fig. 4. A schematic diagram of the orthorhombic BaO_2 layer, superimposed on a hexagonal BaO_2 layer viewed from the [001] direction.

It is worth noting that a number of reports on related perovskites have described difficulties with the refinement of site occupancies and thermal parameters in similar BaO_2 layers. In all of these cases, the refinements were carried out against powder data in hexagonal space groups. These difficulties were attributed to disorder, which could reasonably occur in low temperature phases. But, in light of the results described here, it seems possible that some of these materials may have had similar orthorhombic distortions that were modeled as hexagonal disorder. The symptoms of this type of misassignment would be odd thermal parameters, partial occupancies, unusual bond distances and/or unusual coordination geometries in BaO_2 layers. Unfortunately, true disorder produces similar symptoms.

Recognizing that most structural information on perovskites is derived from powder X-ray diffraction, we found it instructive to calculate the powder patterns for the *Cmcm* structure and the idealized $P6_3/mmc$ structure in order to gauge the likelihood of a similar solution being determined from powder data. Because the subtle orthorhombic distortion did not alter the orthohexagonal cell from 'ideal' axis ratios, no significant new reflections were expected. As anticipated only minor intensity differences in the powder profiles were observed, suggesting that C-centered orthorhombic cell would likely have been missed if it were not for the additional information gleaned from the single crystal data.

The magnetic properties of the $BaFeO_{3-x}$ family vary considerably with oxygen vacancy. Typically, these compounds display antiferromagnetic ordering below

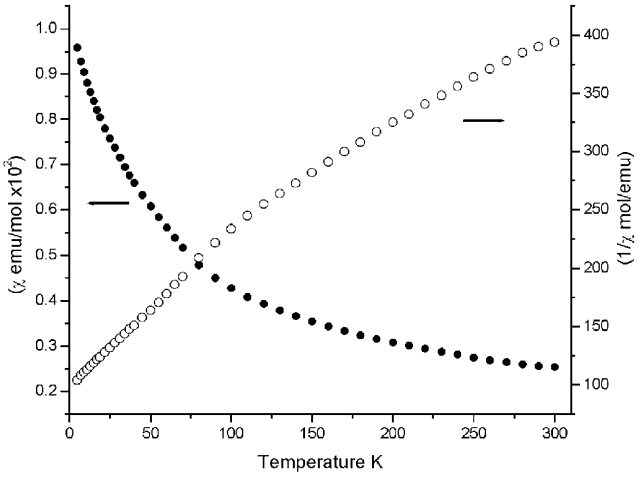

Fig. 5. Plot of χ_{mol} and χ_{mol}^{-1} vs. T for $Ba_5Fe_5O_{14}$ at an applied field of 5000 G.

200°C but Néel temperatures above room temperature have been reported. We have investigated the magnetic properties of $Ba_5Fe_5O_{14}$ from 5 to 300 K using SQUID magnetometry. The molar susceptibility and the inverse molar susceptibility at an applied field of 5000 G are shown in Fig. 5. The inverse susceptibility is nonlinear over the entire range examined and therefore does not exhibit Curie–Weiss behavior. This is indicative of considerable cooperative interaction between the magnetic species which persists above room temperature. The negative temperature intercept observed in $1/\chi$ vs. T plot suggests antiferromagnetic interactions. The overall size of the magnetic moment observed is consistent with antiferromagnetic order above room temperature.

A marked increase in susceptibility at lower temperatures is also observed, which correlates with the downward curvature in the inverse susceptibility plot. This can be attributed to unpaired spins due to stacking faults and other defects. However, the magnetic interactions are predominantly antiferromagnetic at low temperature and might also include magnetic cluster formation. Comparable behavior [31] has been observed in $Ba_5Fe_4Ti_{10}O_{31}$ and was also attributed to the formation of magnetic clusters.

4. Conclusions

Crystals of $Ba_5Fe_5O_{14}$ were precipitated from a molten flux and characterized by single crystal X-ray diffraction and magnetometry. The structure is similar to a previously described 10-layer hexagonal perovskite, but subtle atomic displacements within the oxygen deficient BaO_2 layer away from 6-bar hexagonal sites lowers the symmetry from hexagonal to orthorhombic. The primary structure is trimers of FeO_6 octahedra pillared by dimers of corner-sharing FeO_4 tetrahedra. By comparing the Fe–O bond distances to know compounds, we have determined that the Fe^{4+} atoms are located in the center of the trimer and in the tetrahedral sites, while Fe^{3+} atoms occupy the terminal trimer sites. Magnetic susceptibility measurements indicate that $Ba_5Fe_5O_{14}$ is antiferromagnetic with an ordering temperature above room temperature.

Acknowledgments

The authors thank Dr. Fred Hollander and Dr. Allen Oliver for helpful discussions on twinning. A.M.S. thanks the Committee on Research at UC Berkeley for a Faculty Research Grant.

References

[1] M. Erchak, I. Fankuchen, R. Ward, J. Am. Chem. Soc. 68 (1946) 2085.
[2] W.W. Malinofsky, H. Kedesdy, J. Am. Chem. Soc. 76 (1954) 3090–3091.
[3] H.J. van Hook, J. Phys. Chem. 68 (1964) 3786.
[4] S. Mori, J. Am. Ceram. Soc. 49 (1966) 600.
[5] T. Negas, R.S. Roth, J. Res. Natl. Bur. Stand. A: Phys. Chem. A 73 (1969) 425.
[6] S. Mori, J. Phys. Soc. Jpn. 28 (1970) 44.
[7] M. Zanne, C. Gleitzer, J. Aubry, Bull. Soc. Chim. Fr. (1970) 36.
[8] M. Zanne, C. Gleitzer, Bull. Soc. Chim. Fr. (1971) 1567.
[9] A.J. Jacobson, Acta Cryst. B 32 (1976) 1087–1090.
[10] J.C. Grenier, A. Wattiaux, M. Pouchard, P. Hagenmuller, M. Parras, M. Vallet-Regí, J. González-Calbet, M.A. Alario-Franco, J. Solid State Chem. 80 (1989) 6–11.
[11] M. Parras, M. Vallet-Regí, J.M. González-Calbet, J. Solid State Chem. 83 (1989) 121–131.
[12] M. Parras, M. Vallet-Regí, J.M. González-Calbet, J.C. Grenier, P. Hagenmuller, J. Rodriguez-Carvajal, Euro. J. Solid State Inorg. Chem. 26 (1989) 299–312.
[13] M. Parras, J.M. González-Calbet, M. Vallet-Regí, J.C. Grenier, Solid State Ionics 63–65 (1993) 714–718.
[14] J.M. González-Calbet, M. Parras, M. Vallet-Regí, J.C. Grenier, J. Solid State Chem. 86 (1990) 149–159.
[15] X.D. Zou, S. Hovmoller, M. Parras, J.M. González-Calbet, M. Vallet-Regí, J.C. Grenier, Acta Cryst. A 49 (1993) 27–35.
[16] M.I. Gomez, G. Lucotti, J.A. de Moran, P.J. Aymonino, S. Pagola, P. Stephens, R.E. Carbonio, J. Solid State Chem. 160 (2001) 17–24.
[17] S. Mori, J. Am. Ceram. Soc. 48 (1965) 165.
[18] J.M. González-Calbet, M. Parras, M. Vallet-Regí, J.C. Grenier, J. Solid State Chem. 85 (1990) 15–22.
[19] L. Katz, R. Ward, Inorg. Chem. 3 (1964) 205.
[20] P.D. Vernooy, A.M. Stacy, J. Solid State Chem. 95 (1991) 270–274.
[21] J.L. Delattre, A.M. Stacy, V.G. Young, G.J. Long, R. Hermann, F. Grandjean, Inorg. Chem. 41 (2002) 2834–2838.
[22] XPREP: Part of the SHELXTL Crystal Structure Determination Package, 5.03 Edition, Siemens Industrial Automation, Inc., Madison, WI.
[23] G.M. Sheldrick, SADABS: Siemens/Bruker Area Detector Absorption Correction Program, 2.03 Edition, University of Göttingen, Germany, 1999.

[24] A.L. Patterson, J.S. Kasper, in: International Tables for X-ray Crystallography II, Kynoch Press, Birmingham, UK, 1959, pp. 342–354.
[25] G.S. Zhdanov, Compt. Rend. Acad. Sci. URSS 48 (1945) 39–42.
[26] H.U. Schaller, S. Kemmlersack, A. Ehmann, J. Less-Common Met. 97 (1984) 299–315.
[27] H. Takizawa, H. Steinfink, J. Solid State Chem. 121 (1996) 133–137.
[28] R.D. Shannon, Acta Cryst. A 32 (1976) 751–767.
[29] G. Liu, J.E. Greedan, J. Solid State Chem. 110 (1994) 274–289.
[30] T. Ichida, J. Solid State Chem. 7 (1973) 308–315.
[31] T. Siegrist, T.A. Vanderah, A.P. Ramirez, R.G. Geyer, R.S. Roth, J. Alloys Compd. 274 (1998) 169–178.